Engineering Failure Analysis 93 (2018) 44–54

Contents lists available at ScienceDirect

Engineering Failure Analysis

journal homepage: www.elsevier.com/locate/engfailanal

Short Communication

Seismic behaviour of damaged tunnel during aftershock

D.K. Singh, A. Mandal*, S.R. Karumanchi, A. Murmu, N. Sivakumar

Dept. of Civil Engineering, Visvesvaraya National Institute of Technology, Nagpur 440010, India

ARTICLE INFO

Keywords:
Tunnel
Shake table
Bender element
Aftershock
Damage

ABSTRACT

This paper studies the seismic behaviour of tunnels that are damaged during aftershocks. The tunnels were made from three different materials that had different flexural rigidity. An undamaged tunnel was constructed out of one material, while the damaged tunnels were built with the other two materials. The seismic load was applied with a unidirectional shake table. The peak ground acceleration for various input motions varied from 0.1 g to 1.2 g. The dynamic earth pressure around the tunnel was measured using three soil pressure transducers. The tunnel was placed in the transverse direction of shake table motion. The properties of the surrounding soils were calculated from bender element. The peak dynamic stress generated in the soil was used to study the behaviour of the damaged tunnels. A hand-held vibration analyser was used to measure the motion of the shake table. The results show that the damaged tunnel is more vulnerable to low frequency seismic motion.

1. Introduction

The demand for underground spaces has increased with the increased population. The underground structures were constructed mostly in mountainous region with hard rock strata and with little or few human population. However, during the last few decades, underground structures have been constructed beneath cities with large human populations living in densely packed buildings. Comparatively shallow cover and soft ground conditions make such structures more vulnerable. Thus, any damage to the underground structure beneath the city can cause severe damage to the surrounding structures and human lives. Therefore, the underground structures constructed beneath the city need greater safety and functionality during main shocks (MS) and aftershocks (AS). Aftershocks (AS) are very common phenomena observed after the MS and are believed to follow the Gutenberg-Richter Law. The randomness and large magnitude of AS have the potential to collapse structures damaged during MS. Most often, the larger MS are followed by larger AS [1–6]. Hence, this research focuses on the seismic behaviour of the damaged tunnel during AS.

The severity of earthquakes to underground structures can be seen from the results of the Kanto earthquake, which occurred in year 1923 and damaged about ninety-three tunnels. Twenty-five out of ninety-three tunnels damaged in the Kanto earthquake had to be reconstructed. Also, the ground collapse resulted from lining damage. The Izu-Oshima-Kinkai earthquake damaged nine tunnels that crossed the fault line. The Kobe earthquake in 1995 caused the tunnel lining to fail under shear and compression. In a more recent Niigataken-Chuetsu earthquake in 2004, twenty-four tunnels were damaged. The tunnels near the epicentre (within 10 km radius) sustained heavy damage. Spalling of concrete lining was observed along with a reduction in the tunnel's diameters [7]. The tunnels passing through rock were also damaged during the Niigataken-Chuetsu earthquake [8]. Dowding (1978) collected data about seventy-one (71) tunnels and found that the tunnels are vulnerable to damage only if the peak ground acceleration (PGA) exceeds 0.19 g. Furthermore, PGAs of 0.19 to 0.5 g are moderately damaging and PGAs of 0.5 g or more are heavily damaging [8].

Many researchers have reported that the sections damaged occurred during MS become more vulnerable during AS [9–12].

* Corresponding author.
E-mail address: amandalthesis@yahoo.com (A. Mandal).

https://doi.org/10.1016/j.engfailanal.2018.06.028
Received 20 March 2018; Received in revised form 19 June 2018; Accepted 28 June 2018
Available online 30 June 2018
1350-6307/

However, most studies on structural damage during AS were carried out on buildings [10, 11, 13, 14], bridge piers or reinforced columns [9, 15], and gravity dams [16]. Very few investigated tunnel damage [12]. Soil liquefaction due to AS has also been studied [17]. The effect of frequency of AS on the seismic response of reinforced concrete columns has also been reported [9]. Damage and ductility-based reduction factors have also been used by researchers to quantify the extent of damage to buildings [18]. However, tunnels are confined by surrounding soil, therefore such parameters may not be suitable to quantify the damage of tunnels during AS. In addition, repetitive earthquake loading causes deterioration in mechanical properties of surrounding rock. AS should not be ignored because they can cause further failure of tunnels in soft rock. Moreover, considering AS in the design of the tunnel is important when the tunnel is situated in the Meizoseismal area [12]. Still, no significant work has studied the behaviour of underground structures during AS. Parameter like shear force and bending moment reduction in damaged tunnel, fault movement and change in alignment due to bending of tunnel can affect the behaviour of damaged tunnel. However, shear force and bending moment reduction will have major effect on seismic behaviour of damaged tunnel and this parameter is considered for the present analysis.

Therefore, an experimental investigation to study the seismic behaviour of tunnels during AS is presented in this paper. The experiment was carried out on a tunnel of 15 cm diameter with varying thicknesses. As the tunnel is damaged during main shocks (MS), its shear force and bending moment carrying capacity are reduced. This reduction is simulated by varying the thickness of the tunnel, which changes the flexibility ratio, which is an important criterion governing the seismic behaviour of the tunnel. The tunnel with thickness 1.6 mm ($T_{(t=1.6)}$) and 1.0 mm ($T_{(t=1.0)}$) is 22 and 95 times more flexible compared to a tunnel with thickness 3.0 mm (($T_{(t=3.0)}$)), respectively. The input motion was generated with a shake table, and the tunnel was placed along the transverse direction of the motion. Three soil pressure transducers were used to measure peak dynamic soil pressure. It was found that AS of low frequency has a significant effect on the extent of damage in the tunnel.

2. Methodology

2.1. Shake table test

The experimental work was done on a unidirectional shake table. The size of the shake table top is 1.5 m × 1.5 m. It has a maximum load carrying capacity of 2000 kg. The maximum theoretical frequency is 10 Hz and maximum displacement is ± 50 mm. A rigid container of 18 mm thick perplex glass measuring 1.0 × 1.0 × 1.0 m was mounted on top of the shake table (Fig. 1). The tank is additionally supported by using angle and flat steel sections. The tank base was made rough by gluing sand to it to avoid slippage between the tank and the soil. The vertical boundaries were made absorbent by sticking expanded polyethylene (EPE) foam to them.

2.2. Sensors arrangement

Two types of sensors were used to measure the seismic response of the tunnel. Three soil pressure transducers were used to measure the peak dynamic pressure in the soil. The data were recorded on the dynamic data acquisition module. Fig. 2 shows the arrangements of sensors. The hand-held vibration analyser was used to capture the actual motion of the shake table. The hand-held

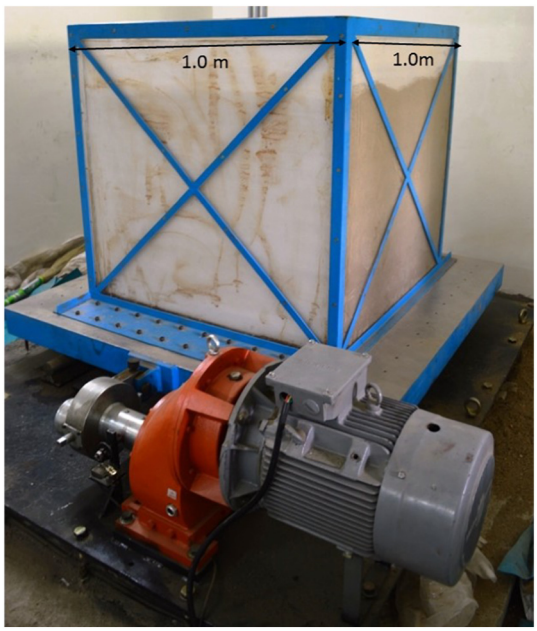

Fig. 1. Shake table with container.

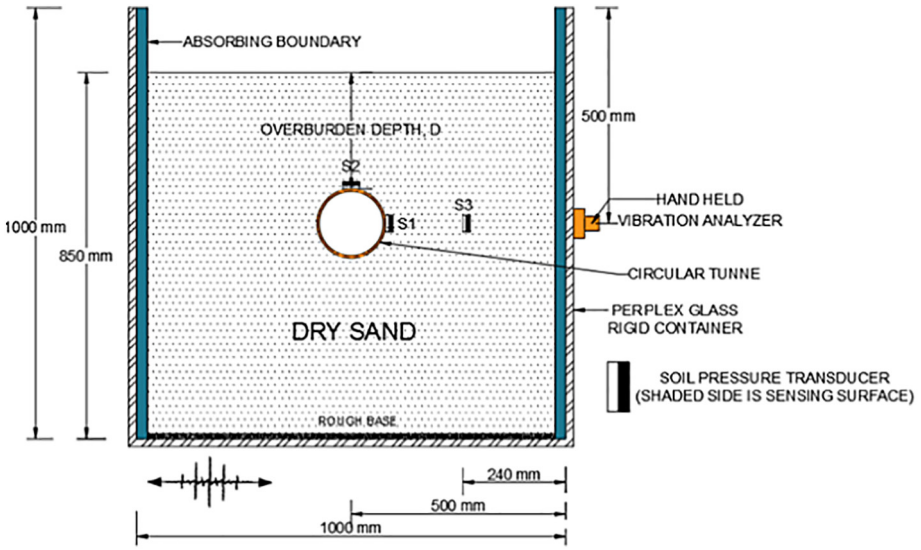

Fig. 2. Experimental setup and arrangement of sensors for transverse direction of tunnel.

vibration sensors with magnetic tip were placed at the centre of the vertical boundary of the container/tank (see Fig. 2).

2.3. Absorbing boundary

To minimize the effect of artificial boundaries, various types of soil containers are developed in past. Based on equivalent shear beam approach flexible soil containers are designed. However, their performance in large deformation experiment is questionable. The laminar box is designed by matching the stiffness of container and soil. Laminar box is extremely useful for large deformation experiments like soil liquefaction. However, during small deformation experiments, they may not replicate the actual boundary conditions [19]. In past several researchers have used rigid containers for 1-g shake table or centrifuge test and suggested to use a soft material to minimize the reflection of waves. In this experiment commercially available EPE foam panel was used as the absorbing boundary in the tests to minimize the boundary effect. The effect of artificial boundaries of a soil container on dynamic response of soil can be significant. For a good absorbing boundary, the impedance of soil should be greater than 200 times the impedance of foam [19]. The thickness of foam for practical use is obtained from Lombardi et al. 2015. For this test, the thickness of foam is 25 mm. These pieces of foam were placed on both inner sides of the end walls of the soil container, perpendicular to the shaking direction. The hysteresis loss of energy in the foam was calculated according to ASTM D 3574–17 to determine the damping (Fig. 3). The compression force displacement (CFD) procedure was followed [20]. Eq. (1) calculates the hysteresis loss and for used EPE foam it is 25%.

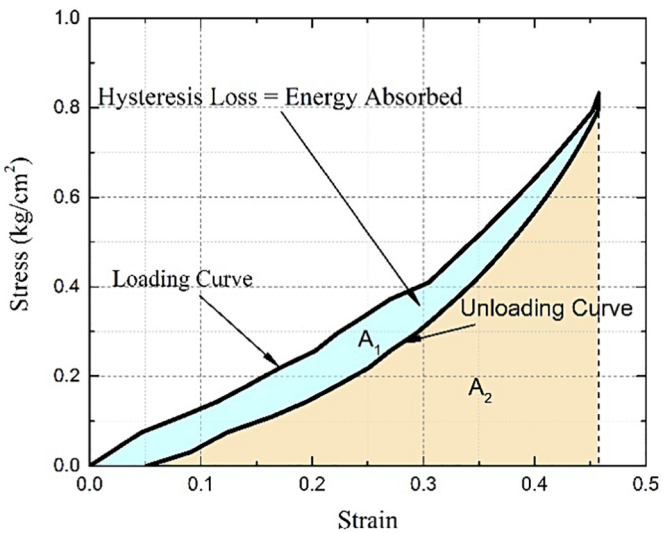

Fig. 3. Hysteresis loss in foam.

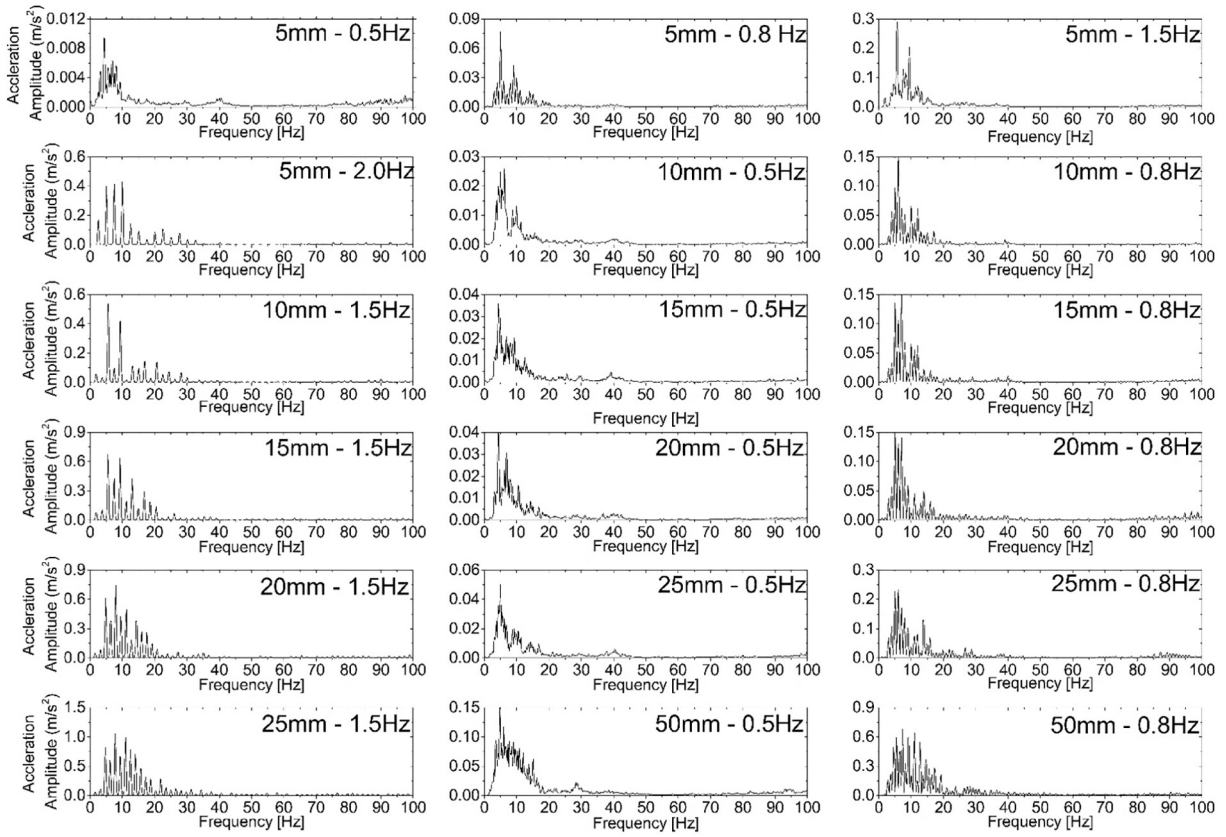

Fig. 4. Frequency spectrum of shake table motion showing frequency and amplitude.

$$\text{Hysteresis loss} = \frac{A_1}{A_1 + A_2} \tag{1}$$

where A_1 is the area in between the loading-unloading curve and A_2 is the area under the unloading curve.

2.4. Input motion

A hand-held vibration analyser was used to capture the actual motion of the shake table. The maximum frequency of 100 Hz was set to capture with intervals of 0.25 Hz. The final data shown by the hand-held vibration analyser are the average of data obtained by 10 cycles of shake table movement. It is assumed that the vibration captured by the hand-held vibration analyser is purely from the shake table, so no filtering of the data is done. The test is performed by changing the shake table's displacement and its frequencies. Fig. 4 shows the frequency spectrum for various motions of the shake table during the test. The same input motion is used for MS and AS. Since the AS can be as strong as the MS [5, 21], the use of the same input motion is justified.

2.5. Material properties

The mechanical properties like Young's modulus, shear modulus and Poison's ratio of coarser fill and foam were calculated using Bender element. P-wave measurement from bender element is much more reliable than S-wave measurement [22]. However, experimental results of Gu et al. to measured shear wave velocity in dry and saturated sand using bender element, resonant column and cyclic torsional shear test shows that the G_{max} values of samples (dry and saturated conditions) prepared by dry tamping are consistent for all the three methods [23]. Also, similar observations were made by other researchers [22, 24–26].

In this test, the p-wave and s-wave velocity are computed by dividing the length of the sample by the time taken by waves to move from the source end to the receiver end. For this test, the sample length was 12 cm and the diameter was 6.0 cm. These dimensions were selected to obtain the best results from bender element tests because a slenderness ratio greater than 2 gives the best results [27]. However, bender element source and receiver ends have outward projections of 1.5 mm each, so tip to tip distance between source and receiver is 11.7 cm. The test was conducted at a density of 1.80 g/cm^3 (Fig. 5a). The specific gravity for coarser fill is 2.80. Also, the value of D_{60}, D_{30} and D_{10} was 5.2 mm, 1.2 mm and 1.0 mm, respectively. The void ratio in loose state (e_{max}) is 0.83, and void ratio in dense state (e_{min}) is 0.49.

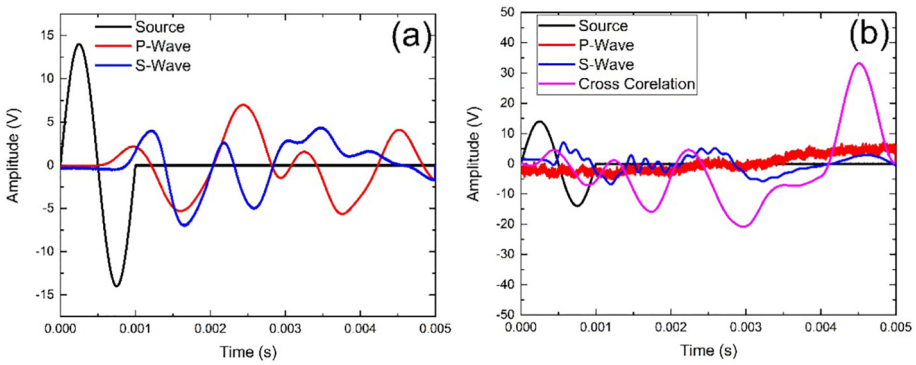

Fig. 5. Bender element test results (a) coarser fill (1.80 g/cm^3), and (b) foam.

The bender element can be used for materials treated with air foam, i.e. the material having a greater quantity of air voids [28]. Here, the tip to tip distance between source and receiver is 6.2 cm. For industrial foam, the s-wave shows the peak clearly. However, the p-wave obtained during the test does not show any peaks (Fig. 5b). Thus, cross correlation can be used to find the p-wave's velocity [29].

Table 1 shows the properties of various materials used in this experiment. Eqs. (2-4) calculate the shear modulus, Poisson's ratio and Young's modulus of the materials, respectively.

$$G = V_S^2 \rho \tag{2}$$

$$v = \frac{\left(\frac{V_p}{V_S}\right)^2 - 2}{2\left(\frac{V_p}{V_S}\right)^2 - 1} \tag{3}$$

$$E = \frac{V_p^2 \rho (1 + v)(1 - 2v)}{1 - v} \tag{4}$$

where G is the shear modulus, ρ is the density of material, V_s is s-wave velocity, ν is the Poisson's ratio, V_p is p-wave velocity and E is Young's modulus.

The value of the soil-tunnel interaction coefficient is calculated by performing the direct shear test. The dimension of the direct shear box is 6 cm × 6 cm and the height is 2.4 cm. A perplex glass plate of thickness 12 mm was placed on the lower side of the direct shear box, and the upper part was filled with the coarser fill with a density of 1.8 g/cm^3. The soil-tunnel interface coefficient of friction from the direct shear test was calculated to be 0.18. A tensile test was conducted on a perplex glass rod of 12 mm diameter to calculate the Young's modulus of the tunnel, this represents material having thickness 3.0 mm. The sample size for tensile test of other two materials having thickness 1.6 mm and 1.0 mm was 15 mm in width and gauge length of 50 mm.

Fig. 6 shows the stress-strain curve for the materials used to make the tunnel. The behaviour of the tunnel with thickness of 3.0 mm was brittle, while the tunnel with thickness of 1.6 mm behaves like quasi-brittle material and the tunnel with thickness 1.0 mm behaved like ductile material.

2.6. Soil placement in container

Coarser fill material was used in the test. During the test, the soil was placed in the container in layers. Permanent changes can appear in internal forces because of densification of sand layers during intense shaking [30]. Also, this will ensure that uniformity is maintained during several dynamic tests. Initially, soil was placed at different densities, and the shake table test was conducted without a tunnel to determine the density at which no settlement in soil occurs. At density 1.8 g/cm^3, the soil settlement is not significant. Hence, this density was selected for further tests.

Table 1
Material properties.

Sr. No.	Material	Density (kg/m^3)	Poisson's Ratio	Young's Modulus (kPa)	c (kPa)	ϕ (°)
1	Coarser Fill	1800	0.27	51,179	0	42
2	Foam	22	0.25	2396	–	–
3	Tunnel$_{(t=3.0)}$	1190	0.37	3,102,640	–	–
4	Tunnel$_{(t=1.6)}$	90	0.40	898,332	–	–
5	Tunnel$_{(t=1.0)}$	90	0.40	876,143	–	–

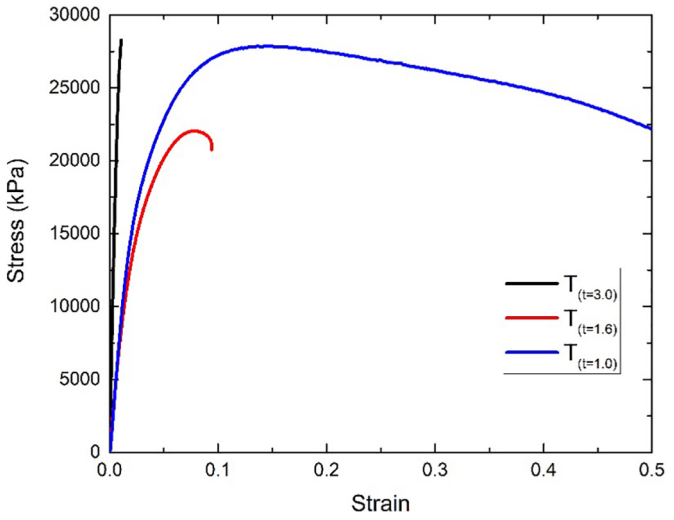

Fig. 6. Stress-strain curve of different materials.

2.7. Experimental tests

The soil container was firmly fixed to the shake table. The dry coarser fill was placed in container in three layers by air pluviation. Additional tamping was done to achieve the desired density (Fig. 7). The tunnels were placed in the soil at an overburden depth/cover of 10 cm perpendicular to the direction of the shake table motion. Fig. 2 shows the arrangement of the sensors. The seismic force was induced by changing the displacement and frequencies of the shake table. For this test, 5 mm displacements have four different frequencies, 0.5, 0.8, 1.5, 2.0 Hz. 10, 15, 20, and 25 mm displacements have three different frequencies of 0.5, 0.8 and 1.5 Hz, whereas for 50 mm displacement, two frequencies 0.5 and 0.8 Hz were used. The dynamic soil pressure generated during each motion was captured.

2.8. Assumptions

- During the main earthquake, the tunnel is damaged to such an extent that its bending moment and shear force carrying capacity are reduced. In reinforced concrete columns, this reduction can be up to 80% [31]. However, no such data are available for the tunnel. The tunnel's behaviour during the main shock can be represented by the case of the tunnel with thickness of 3.0 mm.
- During aftershocks, the resistance to seismic force is developed from reinforcement mesh only; concrete provides no resistance. This can be represented from the tunnel with thickness 1.6 mm and 1.0 mm.
- The sheet is used to make extremely flexible tunnels behave identically to pure reinforcement mesh during seismic loading because the stress-strain curve of these materials is similar to that of reinforcing steel, i.e., ductility is large (Fig. 6). The reinforcement mesh can be represented by using these materials.
- Tunnels at shallow depth are more vulnerable to damage during earthquake than deep tunnels [8]. It is a standard practice of providing weep holes in tunnel just to reduce the water pressure on tunnel lining [32]. This causes lowering of water table in nearby areas [33]. Damage tunnel will have larger cracks which will allow water to pass easily. Also, in this experiment tunnel is

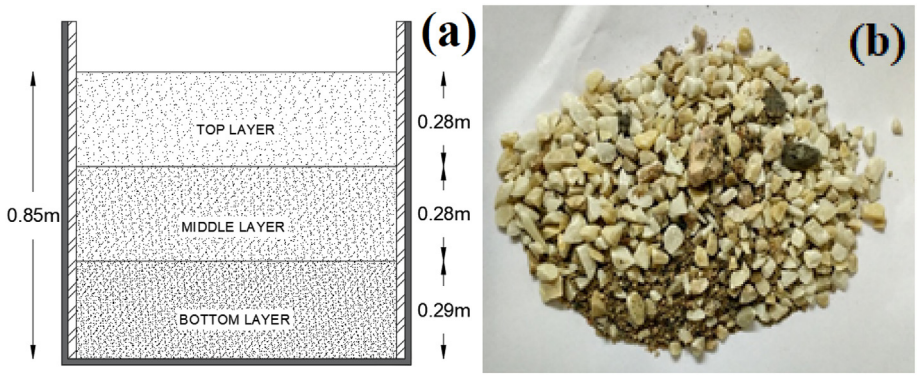

Fig. 7. Coarser fill (a) layer, and (b) material.

Table 2
Flexibility ratio of tunnels in different soil layers with different diameters.

Soil density	Flexibility ratio		
	$T_{(t=3.0)}$	$T_{(t=1.6)}$	$T_{(t=1.0)}$
1.80 g/cm^3	376	8566	35,975

surrounded by coarse sand and water can drain easily. Hence, it is assumed that the effect of pore water pressure on tunnel may not be significant and not considered in this study.

3. Results and discussion

3.1. Flexibility ratio

The relative stiffness between a circular tunnel lining and the soil medium is determined by the flexibility ratio, which is defined by Eq. (5). The ability of the tunnel to resist the distortion imposed from soil medium during seismic load is measured by the flexibility ratio. Table 2 shows the flexibility ratios of three different thicknesses of the tunnel.

$$\text{Flexibility ratio} = \frac{E_s(1\text{-}v_t^2)R^3}{6E_tI(1 + r_m)} \tag{5}$$

where Es = modulus of elasticity of the medium; ν_m = Poisson's ratio of the medium; E_t = modulus of elasticity of the tunnel lining; ν_t = Poisson's ratio of the lining; R = radius of the tunnel lining; t = thickness of the tunnel lining; and I = moment of inertia of the tunnel lining (per unit width).

3.2. Effectiveness of absorbing boundary

The effectiveness of the absorbing boundary was checked by measuring the stresses at two different covers (at 10 cm and 50 cm from the top) in soil without tunnels. The overall depth of the sand layer was 85 cm. Three soil pressure sensors were installed at different distances from the absorbing boundary (at 0 cm, 24 cm and 48 cm). Table 3 shows the results of horizontal stress in the direction of shaking (25 mm displacement with 1.5 Hz frequency), which was recorded to check the effectiveness of the absorbing boundary. There is a ± 5% deviation in the peak dynamic stress value with respect to zero distance from the absorbing boundary, which can be considered insignificant. For shallow cover, the horizontal dynamic stress is more compared to deep cover.

3.3. Peak dynamic stresses

Fig. 8 shows the percentage variation of peak dynamic stresses normalized with respective static stresses against various input motions used for this experiment. With increases in flexibility of the tunnel, the peak dynamic stresses in soil near the tunnel (S_1) increase significantly (Fig. 8a). The vertical dynamic stresses (S_2) also increase with an increase in flexibility ratio. In contrast, there is a significant change in dynamic stresses (S_3) for $T_{(t=1.6)}$ and $T_{(t=1.0)}$ compared to tunnels with thickness $T_{(t=3.0)}$. However, dynamic stresses (S_3) for $T_{(t=1.6)}$ and $T_{(t=1.0)}$ are almost similar (Fig. 8c). This shows that S_3 is independent of the degree of tunnel damage beyond a certain limit.

Since the input motion is periodic, in motions with higher frequencies, stress reversal occurs faster and the system does not have enough time to impose a full load, whereas for lower frequency motions, stress reversal is relatively slow. Thus, in input motion with lower frequency, the system gets enough time to exert pressure on the tunnel before it is reversed. This higher pressure is applied to the tunnel for lower frequency shaking. Consequently, a weaker aftershock can be far more dangerous to a damaged tunnel.

Fig. 9 shows the soil response during dynamic excitation for input motions of 25 mm - 0.5 Hz, 25 mm - 0.8 Hz and 25 mm - 1.5 Hz. In this input motion 25 mm - 1.5 Hz is the most intense, so 25 mm displacement motion is chosen for comparison. With the increase in input frequency, the predominant frequency of dynamic stresses (S_1) also increases in $T_{(t=3.0)}$. The FFT data of sensor S_1 shows that the predominant frequencies are 0.18 Hz, 0.98 Hz and 1.77 Hz, corresponding to input frequencies of 0.5 Hz, 0.8 Hz and 1.5 Hz, respectively. However, for $T_{(t=1.6)}$ and $T_{(t=1.0)}$, the predominant frequencies of stresses are almost same with a value of 0.24 Hz

Table 3
Effectiveness of absorbing boundary by comparing the horizontal stress at different locations.

Sr. No.	Cover	Stress (kPa) at different distances from absorbing boundary		
		0 cm	24 cm	48 cm
1	10 cm	4.23	4.05	4.1
2	50 cm	2.12	2.01	2.04

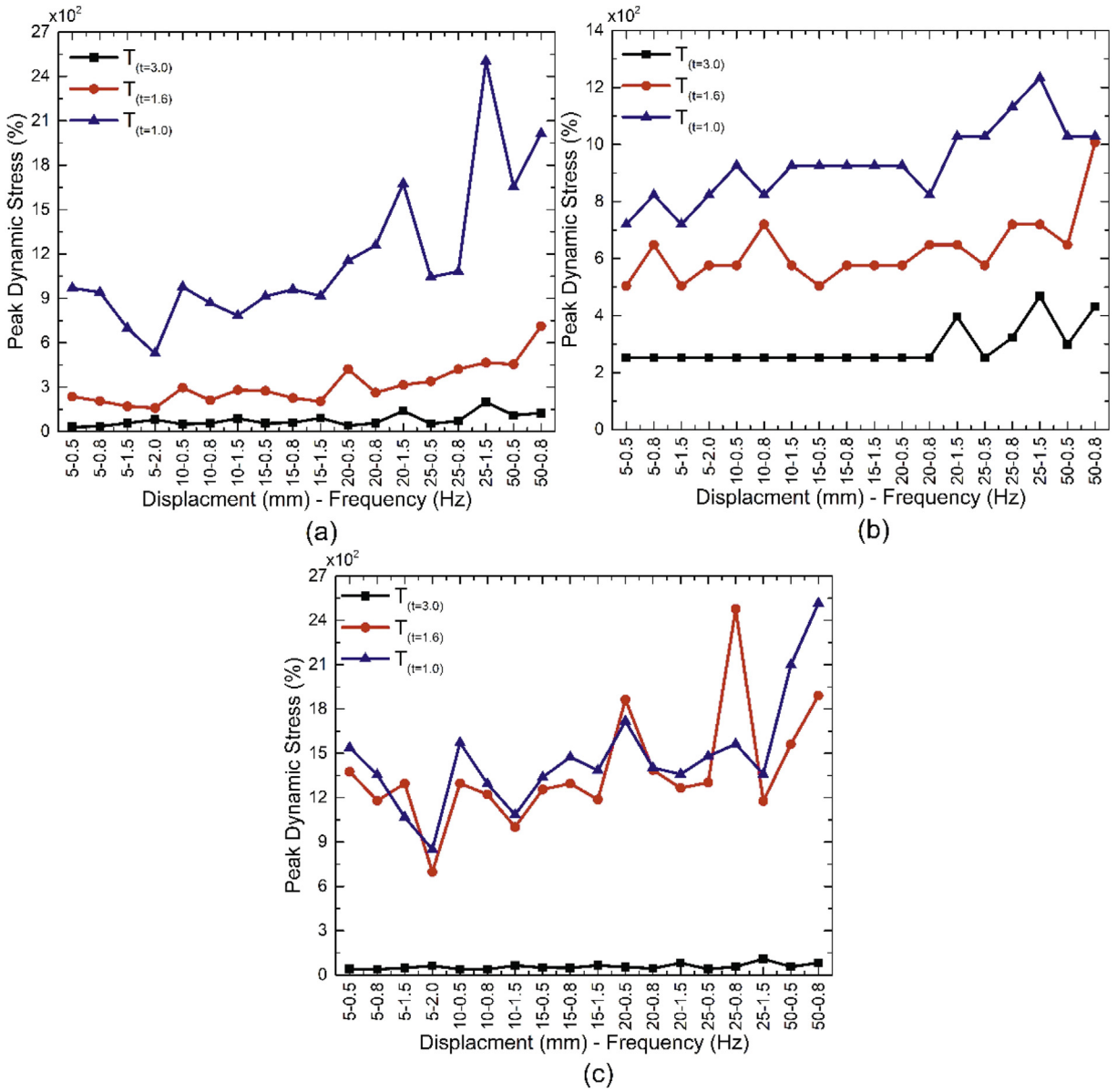

Fig. 8. Peak dynamic stress (%) (a) sensor S_1, (b) sensor S_2, and (c) sensor S_3.

(Fig. 9a) for different input frequencies. The dynamic stress amplitude also increases with increases in input frequencies for $T_{(t=3.0)}$. Whereas for tunnels $T_{(t=1.6)}$ dynamic stress amplitude is approximately 5, for $T_{(t=1.0)}$, it is 16. For damaged tunnels, the dynamic stress amplitude value shows no major change with change in input motion frequencies.

Fig. 9b shows the dynamic stress time history and FFT data of vertical stresses S_2. In tunnel $T_{(t=3.0)}$, input motion frequencies 0.5 Hz and 0.8 Hz have no significant effect on dynamic stresses frequencies. Its value is 0.31 Hz and is same for both the input frequencies. However, for input frequency of 1.5 Hz, there is an increase in dynamic stresses frequencies, in this case, 1.77 Hz. Flexible tunnels $T_{(t=1.6)}$ and $T_{(t=1.0)}$ have no effect of input motion frequencies. The value for S_2 remains same, near 0.24 Hz. Dynamic stress amplitude increases with increase in input motion frequencies for $T_{(t=3.0)}$, whereas it is almost constant for $T_{(t=1.6)}$ and $T_{(t=1.0)}$.

Fig. 9c shows the dynamic stress time history and FFT data of stresses in soil away from tunnel (S_3). The predominant dynamic stress frequency is similar to that of S_1. However, there are changes in values of amplitude. In the case of $T_{(t=3.0)}$, the amplitude of S_3 is less than that of S_1. $T_{(t=1.6)}$, and in the case of $T_{(t=1.0)}$, the amplitude of S_3 is larger than that of S_1.

Fig. 10 shows the condition of the tunnel ($T_{(t=1.0)}$) after the seismic test. A large internal deformation is observed in the tunnel. However, it is interesting to note that the inside deformation of the tunnel is larger at the crown compared to the invert. Also, near the tunnel portals, this inside deformation is less compared to the centre of the tunnel. In a real scenario, an AS can cause huge inside

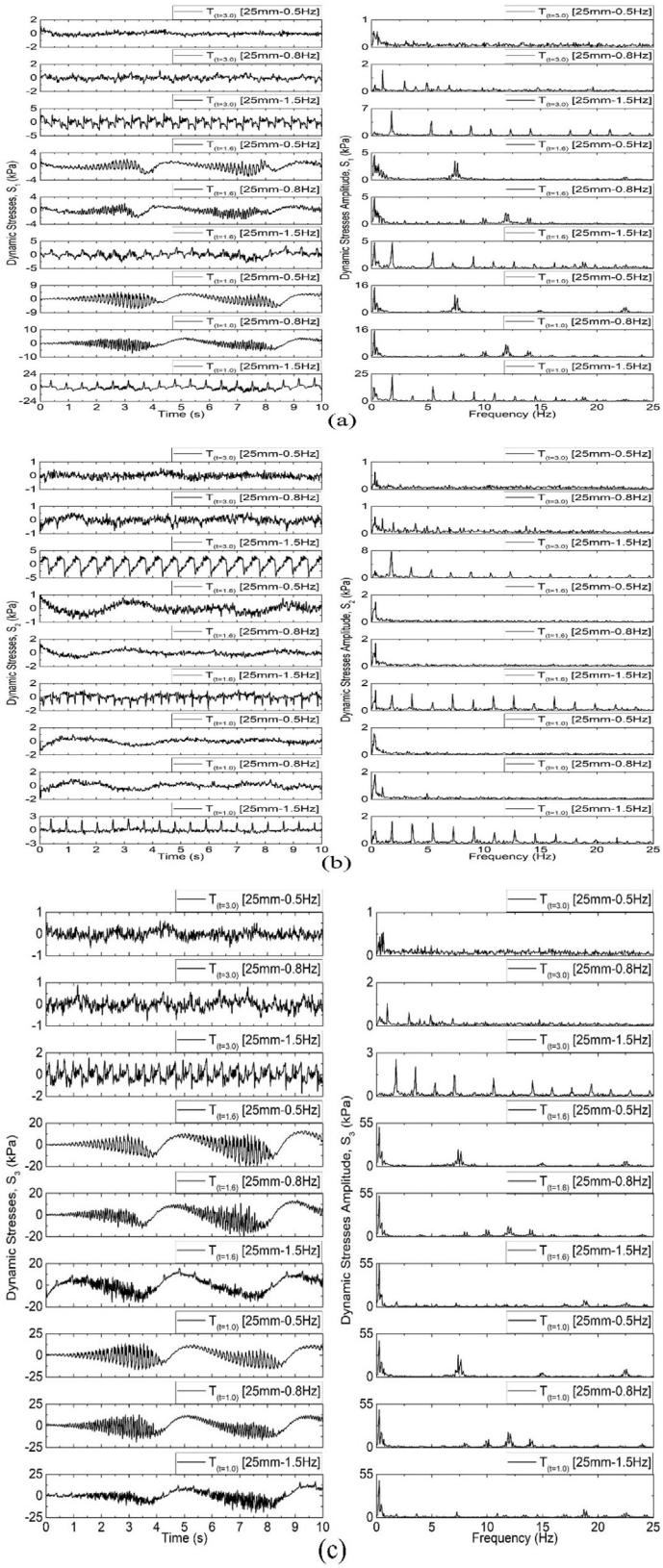

Fig. 9. Soil response for different thickness of tunnels at input motions 25–0.5, 25–0.8 and 25–1.5 (a) dynamic stresses S_1, (b) dynamic stresses S_2, and (c) dynamic stresses S_3.

Fig. 10. $T_{(t=1.0)}$ after test (a) tunnel embedded in soil, and (b) tunnel out of soil.

deformations in a tunnel. This can further affect the nearby structures and cause subsidence on the surface. This demands further detailed study.

4. Conclusion

This paper studied the seismic behaviour of damaged tunnels. It was observed that the damage tunnel is subject to much higher dynamic stress than the undamaged tunnel. Also, lower frequency aftershocks can be more devastating in some conditions. Predominant horizontal dynamic stress frequencies increase with increased input motion frequencies for rigid tunnels. In flexible tunnels, horizontal dynamic stress frequencies do not change much with changes in input frequency. Dynamic stress amplitude is much larger for the flexible tunnel compared to the rigid tunnel. Dynamic stresses in soil away from the tunnel are greater for damaged tunnels compared with undamaged tunnels. Also, it does not depend on the degree of damage.

However, a more detailed study of damaged tunnel behaviours during an earthquake should be conducted. The inside deformation of the tunnel is an important parameter that must be considered to ensure serviceability of underground spaces. Finally, the appropriate non-linear numerical model can be developed to simulate damaged tunnels seismic behaviour.

Acknowledgement

The authors wish to acknowledge the Department of Science and Technology –SERB (Grant No. SB/S3/CEE/0002/2013) for providing the financial support to carry out this research work.

References

[1] J. Ruiz-García, J.D. Aguilar, Influence of modeling assumptions and aftershock hazard level in the seismic response of post-mainshock steel framed buildings, Eng. Struct. 140 (2017) 437–446, http://dx.doi.org/10.1016/j.engstruct.2017.02.074.
[2] G.D. Hatzigeorgiou, A.A. Liolios, Nonlinear behaviour of RC frames under repeated strong ground motions, Soil Dyn. Earthq. Eng. 30 (2010) 1010–1025, http://dx.doi.org/10.1016/J.SOILDYN.2010.04.013.
[3] M. Fragiacomo, C. Amadio, L. Macorini, Seismic response of steel frames under repeated earthquake ground motions, Eng. Struct. 26 (2004) 2021–2035, http://dx.doi.org/10.1016/J.ENGSTRUCT.2004.08.005.
[4] Q. Li, B.R. Ellingwood, Performance evaluation and damage assessment of steel frame buildings under main shock–aftershock earthquake sequences, Earthq. Eng. Struct. Dyn. 36 (2007) 405–427, http://dx.doi.org/10.1002/eqe.667.
[5] B. Kim, M. Shin, A model for estimating horizontal aftershock ground motions for active crustal regions, Soil Dyn. Earthq. Eng. 92 (2017) 165–175, http://dx.doi.org/10.1016/j.soildyn.2016.09.040.
[6] A. Urzua, J.T. Christian, Displacements from the 2014 Iquique M8.2 earthquake and M7.7 aftershock added to a sliding displacement model, J. Geotech. Geoenviron. Eng. 141 (2015) 02814002, , http://dx.doi.org/10.1061/(ASCE)GT.1943-5606.0001238.
[7] K. Yashiro, Y. Kojima, M. Shimizu, Historical earthquake damage to tunnels in Japan and case studies of railway tunnels in the 2004 Niigataken-Chuetsu earthquake, Q. Rep. RTRI. 48 (2007) 136–141, http://dx.doi.org/10.2219/rtriqr.48.136.
[8] C.H. Dowding, A. Rozan, Damage to rock tunnels from earthquake shaking, J. Geotech. Eng. Div. ASCE 104 (1978) 175–191.
[9] M. Shin, B. Kim, Effects of frequency contents of aftershock ground motions on reinforced concrete (RC) bridge columns, Soil Dyn. Earthq. Eng. 97 (2017) 48–59, http://dx.doi.org/10.1016/j.soildyn.2017.02.012.
[10] G. Abdollahzadeh, A. Mohammadgholipour, E. Omranian, Seismic evaluation of steel moment frames under Mainshock–aftershock sequence designed by elastic design and PBPD methods, J. Earthq. Eng. 2469 (2017) 1–24, http://dx.doi.org/10.1080/13632469.2017.1387198.
[11] H.V. Burton, S. Sreekumar, M. Sharma, H. Sun, Estimating aftershock collapse vulnerability using mainshock intensity, structural response and physical damage indicators, Struct. Saf. 68 (2017) 85–96, http://dx.doi.org/10.1016/j.strusafe.2017.05.009.
[12] B. Wang, T. Li, C. He, Y. Zhou, Characteristics, causes and control measures of disasters for the soft-rock tunnels in the Wenchuan seismic regions, J. Geophys. Eng. 13 (2016) 470–480, http://dx.doi.org/10.1088/1742-2132/13/4/470.
[13] S. Casolo, A numerical study on the cumulative out-of-plane damage to church masonry façades due to a sequence of strong ground motions, Earthq. Eng. Struct. Dyn. 46 (2017) 2717–2737, http://dx.doi.org/10.1002/eqe.2927.
[14] G. Lanzo, A. Pagliaroli, Numerical modeling of site effects at San Giuliano di Puglia (Southern Italy) during the 2002 Molise seismic sequence, J. Geotech. Geoenviron. Eng. 135 (2009) 1295–1313, http://dx.doi.org/10.1061/(ASCE)GT.1943-5606.0000055.
[15] M.N. Sheikh, F. Légeron, A checking method for multiple seismic performance objectives of bridge Piers designed according to code provisions, J. Earthq. Eng. 20 (2016) 1148–1168, http://dx.doi.org/10.1080/13632469.2015.1118709.
[16] G. Wang, Y. Wang, W. Lu, P. Yan, W. Zhou, M. Chen, Damage demand assessment of mainshock-damaged concrete gravity dams subjected to aftershocks, Soil Dyn. Earthq. Eng. 98 (2017) 141–154, http://dx.doi.org/10.1016/j.soildyn.2017.03.034.

[17] S. Wahyudi, J. Koseki, T. Sato, G. Chiaro, Multiple-liquefaction behavior of sand in cyclic simple stacked-ring shear tests, Int. J. Geomech. 16 (2016) C4015001, , http://dx.doi.org/10.1061/(ASCE)GM.1943-5622.0000596.
[18] Y. Zhang, J. Chen, C. Sun, Damage-based strength reduction factor for nonlinear structures subjected to sequence-type ground motions, Soil Dyn. Earthq. Eng. 92 (2017) 298–311, http://dx.doi.org/10.1016/j.soildyn.2016.10.002.
[19] D. Lombardi, S. Bhattacharya, F. Scarpa, M. Bianchi, Dynamic response of a geotechnical rigid model container with absorbing boundaries, Soil Dyn. Earthq. Eng. 69 (2015) 46–56, http://dx.doi.org/10.1016/j.soildyn.2014.09.008.
[20] ASTM D3574–17, Standard Test Methods for Flexible Cellular Materials—Slab, Bonded, and Molded Urethane Foams, ASTM International, West Conshohocken, PA, 2017, http://dx.doi.org/10.1520/D3574-17.
[21] J. Ruiz-García, Mainshock-aftershock ground motion features and their influence in Building's seismic response, J. Earthq. Eng. 16 (2012) 719–737, http://dx.doi.org/10.1080/13632469.2012.663154.
[22] J. Kumar, B.N. Madhusudhan, A note on the measurement of travel times using bender and extender elements, Soil Dyn. Earthq. Eng. 30 (2010) 630–634, http://dx.doi.org/10.1016/j.soildyn.2010.02.003.
[23] X. Gu, J. Yang, M. Huang, G. Gao, Bender element tests in dry and saturated sand: signal interpretation and result comparison, Soils Found. 55 (2015) 951–962, http://dx.doi.org/10.1016/j.sandf.2015.09.002.
[24] T. Qiu, Y. Huang, Y. Guadalupe-Torres, C.D.P. Baxter, P.J. Fox, Effective soil density for small-strain shear waves in saturated granular materials, J. Geotech. Geoenviron. Eng. 141 (2015) 1–11, http://dx.doi.org/10.1061/(ASCE)GT.1943-5606.0001334.
[25] Y. Cai, Q. Dong, J. Wang, C. Gu, C. Xu, Measurement of small strain shear modulus of clean and natural sands in saturated condition using bender element test, Soil Dyn. Earthq. Eng. 76 (2015) 100–110, http://dx.doi.org/10.1016/j.soildyn.2014.12.013.
[26] J.-U. Youn, Y.-W. Choo, D.-S. Kim, Measurement of small-strain shear modulus G_{max} of dry and saturated sands by bender element, resonant column, and torsional shear tests, Can. Geotech. J. 45 (2008) 1426–1438, http://dx.doi.org/10.1139/T08-069.
[27] J. Camacho-Tauta, J.D. Álvarez-Jiménez, O.J. Reyes-Ortiz, A procedure to calibrate and perform the bender element test, DYNA 79 (2012) 10–18.
[28] S. Kataoka, T. Kawaguchi, ... , T.H.-P. of I., undefined 2011, Unconfined compression strength and elastic shear modulus of air-form treated lightweight soil, 5th International Symposium on Deformation Characterization of Geomaterials, Seoul, 2011, pp. 682–686.
[29] T. Ogino, T. Kawaguchi, S. Yamashita, S. Kawajiri, Measurement deviations for shear wave velocity of bender element test using time domain, cross-correlation, and frequency domain approaches, Soils Found. 55 (2015) 329–342, http://dx.doi.org/10.1016/J.SANDF.2015.02.009.
[30] G. Lanzano, E. Bilotta, G. Russo, F. Silvestri, Experimental and numerical study on circular tunnels under seismic loading, Eur. J. Environ. Civ. Eng. 19 (2015) 539–563, http://dx.doi.org/10.1080/19648189.2014.893211.
[31] J. Zhou, M. Hirosawa, T. Konda, S. Yasushi, Effect of the torsional moment on the shear strength of reinforced concrete columns due to eccentric jointing of beam to column, 12th World Conference on Earthquake Engineering, 2000.
[32] H. Sang Jung, Y. Su Han, S. Rae Chung, B. Sik Chun, Y.J. Lee, Evaluation of advanced drainage treatment for old tunnel drainage system in Korea, Tunn. Undergr. Space Technol. 38 (2013) 476–486, http://dx.doi.org/10.1016/j.tust.2013.08.004.
[33] C. Yoo, Y.J. Lee, S.H. Kim, H.T. Kim, Tunnelling-induced ground settlements in a groundwater drawdown environment - a case history, Tunn. Undergr. Space Technol. 29 (2012) 69–77, http://dx.doi.org/10.1016/j.tust.2012.01.002.

Notations

A_1: area in between loading-unloading curve;
A_2: area under unloading curve;
E: Young's modulus;
E_s: modulus of elasticity of the medium;
E_t: modulus of elasticity of the tunnel lining;
G: shear modulus;
I: moment of inertia of the tunnel lining (per unit width);
R: radius of the tunnel lining;
t: thickness of the tunnel lining;
V_p: p-wave velocity;
V_s: s-wave velocity;
ν: Poisson's ratio;
ν_m: Poisson's ratio of the medium;
ν_t: Poisson's ratio of the tunnel;
ρ: density of material